Carbohydrate Polymers 110 (2014) 156–162

Contents lists available at ScienceDirect

Carbohydrate Polymers

journal homepage: www.elsevier.com/locate/carbpol

Impact of ghosts on the viscoelastic response of gelatinized corn starch dispersions subjected to small strain deformations

H. Carrillo-Navas*, G. Avila-de la Rosa, D. Gómez-Luría, M. Meraz, J. Alvarez-Ramirez, E.J. Vernon-Carter

Departamento de Ingeniería de Procesos e Hidráulica, Universidad Autónoma Metropolitana-Iztapalapa, Apartado Postal 55-534, México, DF 09340, Mexico

ARTICLE INFO

Article history:
Received 28 February 2014
Received in revised form 25 March 2014
Accepted 26 March 2014
Available online 5 April 2014

Keywords:
Gelatinized corn starch dispersions
Small strain deformations
Viscoelasticity
Ghosts
Microstructure

ABSTRACT

Corn starch dispersions (5.0% w/w) were gelatinized by heating at 90 °C for 20 min using gentle stirring. Under these conditions, ghosts, which are insoluble material with high amylopectin content, were detected by optical microscopy. Strain sweep tests showed that the gelatinized starch dispersions (GSD) exhibited a loss modulus (G'') overshoot at relatively low strains (~1%). In order to achieve a greater understanding as to the mechanisms giving rise to this uncharacteristic nonlinear response at low strains, very small constant torques (from 0.05 to 0.5 μN m) were applied in the bulk of the GSD with a rotating biconical disc. This resulted in small deformations exhibiting torque-dependent inertio-elastic damped oscillations which were subjected to phenomenological modelling. Inertial effects played an important role in the starch mechanical response. The model parameters varied with the magnitude of constant small applied torque and could be related to microstructural changes of ghosts and to the viscoelastic response of GSD.

1. Introduction

Gelatinized starch dispersions (GSD) are widely used in the food industry as fat-replacers and thickening agents. The attractiveness of starch gels as food material relative to other polysaccharides (e.g., pectin, gum Arabic, etc.), is their high availability and sustainability from many botanical sources, and their relatively low production costs. GSD can be easily produced by departing from an aqueous starch slurry and heating to temperatures of about 90 °C and higher for relatively short times (20–30 min). As a result, the viscoelasticity of a material can be tailored, via starch type, concentration and processing conditions, for inducing desired texture in food matrices. During the heating process, starch granules are partially dissolved due to swelling-leaching of the amylose molecules and small amounts of amylopectin into the aqueous phase (Biliaderis, Maurice, & Vose, 1980; Ratnayake & Jackson, 2007). The viscoelastic properties of GSD play a central role on the stability and consumers acceptability of food products, such as yoghourt, cheese and emulsions (Muadklay & Charoenrein, 2008; Seetapan et al., 2013).

The cooking temperature largely determines the microstructure of GSD. For relatively high temperatures, above 120 °C, all semi-crystalline and amorphous material contained in the starch granule is dissolved, leading to a homogeneously micro-structured gel. However, under gently shear conditions and at moderate temperatures (about 90–110 °C) that are commonly used in restaurants and industrial food processing plants, the starch granules are not fully dissolved. Despite the solubility of some granule components, remnants of the starch granules, commonly known as ghosts, persist after cooking under mild to moderate shear conditions (Fannon & BeMiller, 1992). The starch ghosts are formed when the hydrated granules burst and collapse (Hoseney, Atwell, & Lineback, 1977) and are composed mostly of amylopectin. Interestingly, ghosts are commonly found in starch pastes that are considered fully gelatinized (Atkin, Abeysekera, Cheng, & Robards, 1998). Ghosts are elastic structures heterogeneously distributed within the continuous viscous matrix (Ratnayake & Jackson, 2007). In this way, the presence of ghosts can have an important effect on the viscoelastic properties of GSD.

The heterogeneous nature of GSD containing ghosts can lead to significant microstructural changes under shear disturbances. Under industrial conditions, GSD are subjected to severe shear conditions where nonlinear viscoelasticity can appear due to gel fractures and ghosts destruction. Large-amplitude oscillatory shear (LAOS) tests can be used for characterizing the mechanical response of GSD under stringent flow conditions (Hyun et al., 2011). In contrast, the viscoelastic properties of GSD under the application of

* Corresponding author. Tel.: +52 55 5804 4934; fax: +52 55 5804 4934.
E-mail address: hcnavas@gmail.com (H. Carrillo-Navas).

http://dx.doi.org/10.1016/j.carbpol.2014.03.088
0144-8617/

mild shear stresses play an important role under shelf and consumption conditions (Carini, Curti, Littardi, Luzzini, & Vittadini, 2013; Cui, Lu, Tan, Wang, & Li, 2014).

A close understanding of the effect of ghosts in the rheological properties of GSD should provide valuable information for the optimal design of food products involving starches. In fact, rheological properties play an important role in the behaviour of GSD under shelf and flow conditions. In this way, the aims of this paper were to study the viscoelastic response of GSD subjected to dynamic shear strain sweep and small constant shear stresses and to establish an interrelationship between the model parameters with the microstructural changes of ghosts and viscoelastic response of GSD.

2. Materials and methods

2.1. Materials

Corn starch (S-4126) was purchased from Sigma–Aldrich (Toluca, State of Mexico, Mexico). The amylose content reported by the provider was 25.03 ± 0.62 g/100 g. The amylose content determined by the Hoover and Ratnayake (2002) test was 25.78 ± 0.57 g/100 g, agreeing well with the value specified by starch provider. Deionised water was used in all the experiments.

2.2. Preparation of GSD

GSD were prepared by suspending the starch (5.0% w/w) in deionised water and heating at 90 °C for 20 min to allow gelatinization of the starch granules. For preserving the integrity of granule remnants, low mixing conditions (150 rpm) were carried out with the help of a magnetic stirrer (Cole-Parmer model 04807, Chicago, IL, USA, stir bar 08546-00 3 mm × 10 mm). The temperature was continuously measured with a Cole-Parmer Scientific Thermistor Thermometer (with USB-W-90080-09; resolution of 0.001 °F/°C) at different points of the dispersion for monitoring heating heterogeneities, showing spatial differences of about ±0.15 °C. The swollen suspensions were then cooled down to 25 °C with the help of a controlled water bath by using a cooling rate of 2.0 °C/min, and immediately used for rheological measurements.

2.3. Optical micrographs

Micrographs of the GSD were taken using an optical microscope (Olympus BX45, Olympus Optical Co., Ltd., Tokyo, Japan) and images were captured with Olympus E-620 digital camera. Samples were put on viewing slides, upon which coverslips were gently placed. The coverslip was previously humidified for reducing the risk of trapping air bubbles. Iodine treatment was used to study the structure of the starch dispersions since iodine diffuses inside amylose-rich regions, forming a deep blue colour inclusion complex. In contrast, spatial regions with low-amylose content retain the characteristic iodine brownish colour.

2.4. GSD sonication

An Ultrasonic Processor (model UP400S, Hielscher Ultrasonics GmbH, Teltow, Germany) at 50% amplitude and frequency of 24 kHz with a 7 mm diameter tip during 10 s, was used for partially destroying the ghost structure of GSD.

2.5. Rheological measurements

2.5.1. Strain sweep tests

Dynamic oscillatory measurements of the GSD were carried out using a Physica MCR 300 rheometer (Physica Meβtechnik GmbH, Stuttgart, Germany), with a cone-plate geometry, in which the rotating cone was 50 mm in diameter, and cone angle of 2° with a gap of 0.05 mm. About 1.25 mL of sample was carefully placed in the measuring system, and left to rest for 10 min at 25 °C for structure recovery. Amplitude sweeps were carried out, with strain ranging from 0.05 to 1000% at 1 Hz. Measurements were performed at 25 °C and temperature maintenance was achieved with Physica TEK 150P Peltier system. The storage modulus (G') and the loss modulus (G'') were obtained from the equipment software (US200/32 V2.50) in all cases. Analysis was performed by triplicate.

2.5.2. Constant shear stress tests

The determination of the shear strain in the bulk of the GSD in response to a different constant torques (0.05–0.5 μN m) application was based on the procedure described by Carrillo-Navas, Fouconnier, Vernon-Carter, and Alvarez-Ramirez (2013) with slight modifications. A Physica MCR 300 (Physica Meβtechnik GmbH, Stuttgart, Germany) modular compact rheometer with a thermosttated acrylic vessel with inner radius, R_c, of 27 mm, inserted in the measuring plate of the rheometer, and coupled to a stainless steel biconical disc geometry, of radius R_b equal to 15 mm and double angle 2α of 10°, was used. GSD was filled into the thermosttated vessel to a height of 12 mm. A laboratory Julabo F25-ME recirculating water bath (Julabo GmbH, Seebach, Germany) was used for maintaining the temperature in the thermosttated vessel from below. Once the GSD had been equilibrated at 25 °C, the rheometer motor drive was slowly lowered so that the stainless steel biconical disc was submerged to a depth of 6 mm within the dispersion bulk. The GSD was immediately subjected to a constant torque (M) during 20 s. The change in the angular displacement of the disc with time (θ_b) was monitored every 0.1 s with the rheometer software. The signals M and θ_b were converted to shear stress (σ_0) and shear strain ($\gamma(t)$) via suitable relationships (Martin, Bos, Stuart, & van Vliet, 2002).

2.6. Numerical fitting of experimental data

Mechanical analogues were used for the phenomenological modelling of the experimental data. This approach resulted in nonlinear second-order differential equations with several parameters (e.g., inertia, viscosity and elasticity modulus) to be numerically estimated. To this end, a standard least-square problem was posed and numerically solved with a FORTRAN code tailored for this work. A 4/5 Runge–Kutta method with constant integration step of 10^{-3} s, was used.

2.7. Statistical analyses

Data were analyzed using a one way analysis of variance (ANOVA). All experiments were done in triplicate.

3. Results and discussion

3.1. Gelatinized starch dispersion microstructure

Aqueous starch dispersions become increasingly viscous when heated at temperatures non-higher than about 90 °C, due to swelling of granules and to leaching of amylose and small amounts of amylopectin into the continuous aqueous phase (McClements, 1999). After the gelatinization process, starch granules can persist in swollen hydrated forms known as ghosts (Ratnayake & Jackson, 2007). A recent study has shown that these granule remnants form when the hydrated granules burst and collapse (Zhang, Dhital, Flanagan, & Gidley, 2014), being comprised mostly by amylopectin (Atkin et al., 1998; Debet & Gidley, 2007). To show this, Fig. 1 presents a light microscopy image of the iodine stained GSD. Brown colour domains correspond to the amylopectin-rich

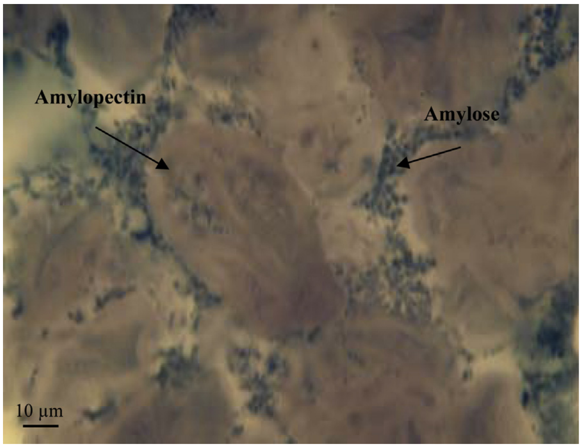

Fig. 1. Iodine strained image (100×) showing the distribution of amylose- and amylopectin-rich regions in GSD. The former corresponds to blue colour, while the latter to brown colour. (For interpretation of the references to color in figure legend, the reader is referred to the web version of the article.)

ghosts that were not solubilized at the temperature (90 °C) and stirring (150 rpm) conditions, while blue colour regions correspond to the gelatinized, amylose-rich, viscous matrix. The spatial domains of the remnant granules can be also observed by normal light microscopy imaging and its binarized version, as shown in Fig. 2a and b. Compactly packed local domains can be noted, indicating that granule remnants formed irregular spatial geometries, possibly caused by the particular combination of a viscous continuous matrix and disperse elastic ghost remnants (Debet & Gidley, 2007). It has been argued that starch dispersions are able to rearrange themselves for adapting to flow conditions and avoiding fracture (Luyten & van Vliet, 1995). The irregular geometric distribution of granule remnants can persist under mild and moderate shear conditions; although their destruction can be induced by relatively high shear rates and heating temperatures (Ghiasi, Hoseney, & Varriano-Marston, 1982; Ratnayake & Jackson, 2007). To illustrate this, the GSD was subjected to short-time (10 s) sonication at 50% amplitude. The idea was to induce remnants disaggregation without severe destruction of the ghosts. Fig. 2c and d shows that the stronger shear conditions induced partial destruction of the ghost configuration. In fact, the binarized image (Fig. 2d) shows that ghost domains were not any longer compactly packed; and that this restructuring could have an important impact on the rheological response of the GSD.

3.2. Strain sweep tests

In this subsection, the results from the experimental strain sweeps tests at 1 Hz will be discussed. Firstly, some insights on the viscoelasticity of GSD will be obtained. Secondly, the results obtained will serve for motivating the estimation of viscoelasticity under inertio-elastic oscillations.

It should be mentioned that a linear viscoelastic region is commonly reported for complex fluids, such as our GSD, at relatively small strains, followed by a nonlinear viscoelastic region at higher strains. This is probably due to the fact that the experimental results are usually plotted in a log–log format, so that small variations in G' and G'' at small strains can be masked. For this reason, the results of the strain sweep test were plotted in a semi-log format (Fig. 3), in order to avoid the scaling effect of the log–log format and for achieving a better visualization of the variations at low strain amplitudes. In the range from 0.05 to 1000%, G' displayed a monotonous decreasing behaviour, indicative of a gradual reduction of the GSD elasticity. In turn, G'' exhibited a non-monotonous behaviour with two overshoots at strains occurring at about 1 and 48%, respectively. Strain overshoots have been observed for biopolymer solutions forming weak microstructural complexes similar to that

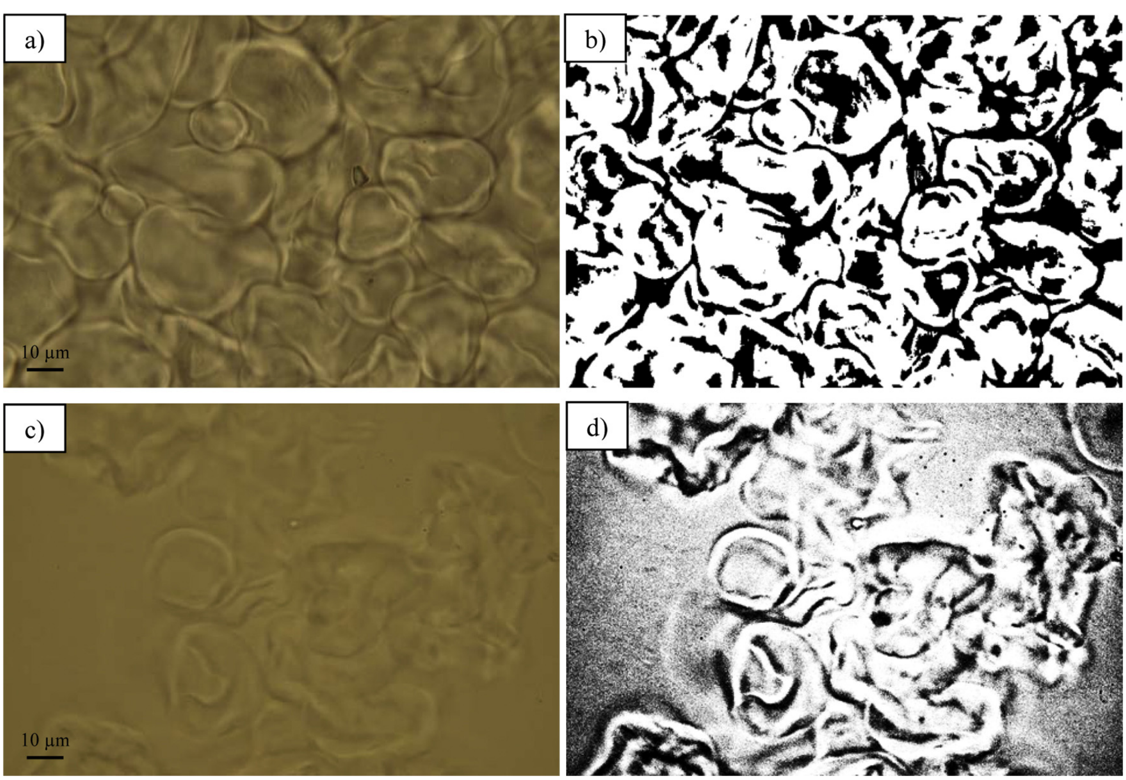

Fig. 2. Example of optical micrograph (100×) of the GSD. Upper panel, (a) and (b), corresponds to GSD prepared under mild stirring conditions, while lower panel, (c) and (d), corresponds to the same GSD after applying short-time sonication (10 s at 50% amplitude).

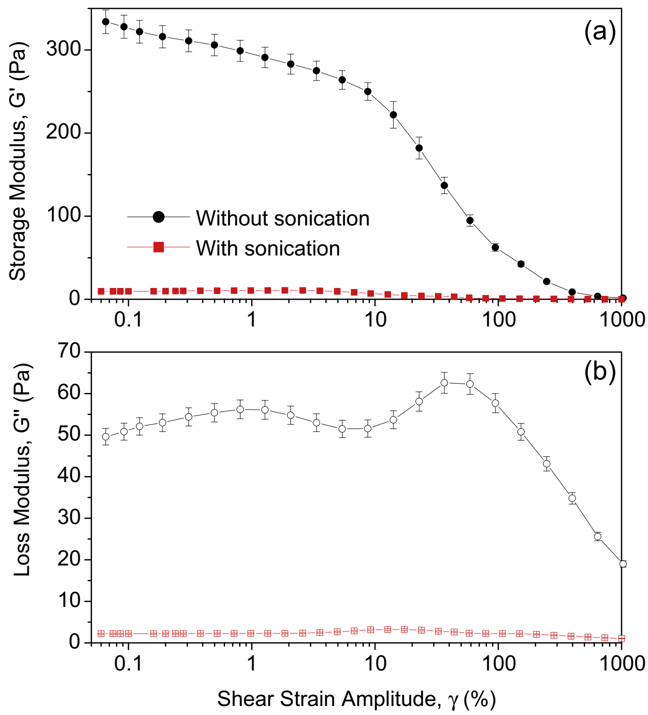

Fig. 3. (a) Storage and (b) loss moduli obtained from strain sweep tests for the GSD. The lack of a linear regime for small deformations is apparent. Also, two strain overshoots in the loss modulus at small and large deformations can be observed.

exhibited by our GSD in Fig. 3 (Hyun, Kim, Ahn, & Lee, 2002). Strain G'' overshoots usually occur when weak structural complexes are formed, as occurs suspensions of flocculated particles (Rochefor & Middleman, 1987). When an external strain is imposed, the complex structure resists against deformation up to a certain strain, where G'' increases. Then the complex structure is destroyed by large deformation to a certain strain, after which the microstructure segments align with the flow field, and G'' decreases (Hyun et al., 2002). Weak strain overshoots have been reported for gelatinized starch dispersions from different botanical origin at relatively high strains (~50%), probably caused by the large deformation of the ghost granules (Hernández-Jaimes, Bello-Pérez, Vernon-Carter, & Alvarez-Ramirez, 2013), which are highly flexible and fragile structures (Debet & Gidley, 2007). That is, the application of increasingly larger shear strains led to jamming and breakage of ghosts in the starch gels. The existence of the smaller overshoot at about 1% strain has not been reported previously to our knowledge. In dispersions, such as ours, where suspended particles are close enough to interact with each other through hydrodynamic interactions, colloidal interactions, or entanglement, flocculation may lead to the formation of a three-dimensional network of aggregated particles (Pal, 1996). Flocs formed by the aggregation of suspended particles often have structures that are fractal. The effective volume fraction of a fractal floc is related to the size of the floc and the fractal dimension (Bremer, Bijsterbosch, Waltra, & van Vliet, 1993). At a given actual volume fraction, when very small shear strains are applied, flocs are driven together, increasing their size, and producing an increase in viscosity. Once a critical strain is exceeded, and the forces holding together the flocs are disrupted, flowing past one another, causing a decrease in viscosity. If some bonds are capable of reforming as shear strain increases, structural reorganization of the flocs takes place leading to the appearance of the G'' overshoot occurring at relatively high shear strain (McClements, 1999). Also, results based on network models have indicated that the overshoot behaviour of G'' is associated with the balance of formation and destruction of network junctions (Sim, Ahn, & Lee, 2003).

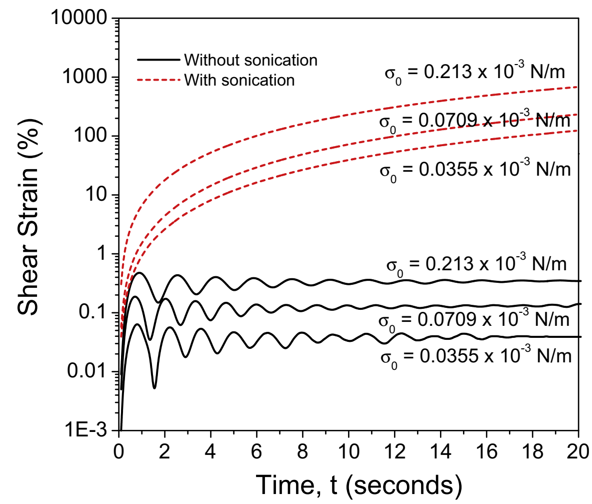

Fig. 4. Examples of shear strain response for three different shear stress values. The oscillations were caused by inertio-elastic effects found when relatively small shear stress values were used.

The relevant feature for the analysis that follows is the lack of a linear regime for small strain amplitudes. The modulus change was about −14.5% for G' and of +28.0% for G'' over the amplitude range from 0.05% to 2%. In general, it is expected that nonlinearities are displayed at relatively large strain amplitudes (Hyun et al., 2011). However, the results in Fig. 3 suggest that nonlinear viscoelasticity responses can be present even at relatively small strain amplitudes. The nonlinearity mechanism should be different for the low and the high-amplitude regimes. Small strains affected little or moderately the gel microstructure, while large strains disrupted it more severely, as depicted in Fig. 3. In line with previous reports (Lourdin, Valle, & Colonna, 1995; Ratnayake & Jackson, 2007), Fig. 2c and d shows that severe shear rate conditions can destroy partially or totally ghost granules, leading to a reduction of the dispersion heterogeneity. Fig. 3 also presents the strain sweep test results for the starch dispersion prepared at 1500 rpm. The rheological response, as represented by the magnitude of the storage and the loss modulus, exhibited a severe depletion and the strain overshoot at about 1% is not longer displayed. This shows that the starch ghosts flocs three-dimensional network and flocs packing were the main factors affecting the viscoelastic response shown by the starch dispersion prepared under mild stirring conditions.

3.3. Constant shear stress tests

Experimental runs were performed by applying small torques for reducing the affectation of the GSD microstructure due to shear stress actions. The applied torque of 0.05 μN m was near the lower limit of the rheometer range (0.02–150 μN m with resolution of 0.002 μN m). In this way, the mechanical response due to the application of small increasing shear stress steps could provide insights regarding the equilibrium viscoelasticity of GSD. The resulting shear strain response is exemplified in Fig. 4 for three different shear stress values. For better visualization, only the mean value of three experimental runs for each applied torque was displayed. As expected, the larger the shear stress applied, the larger the shear strain produced (i.e., the larger the angular displacement of the biconical disc). In all cases, the shear strain displayed damped oscillatory response that converged to a nearly asymptotic value after certain relaxation time. The oscillatory response was dependent of the shear stress value. The first maximum of the shear strain response can be seen as an indicator of the gel elasticity. Under the application of an increasing shear stress step, the GSD responded

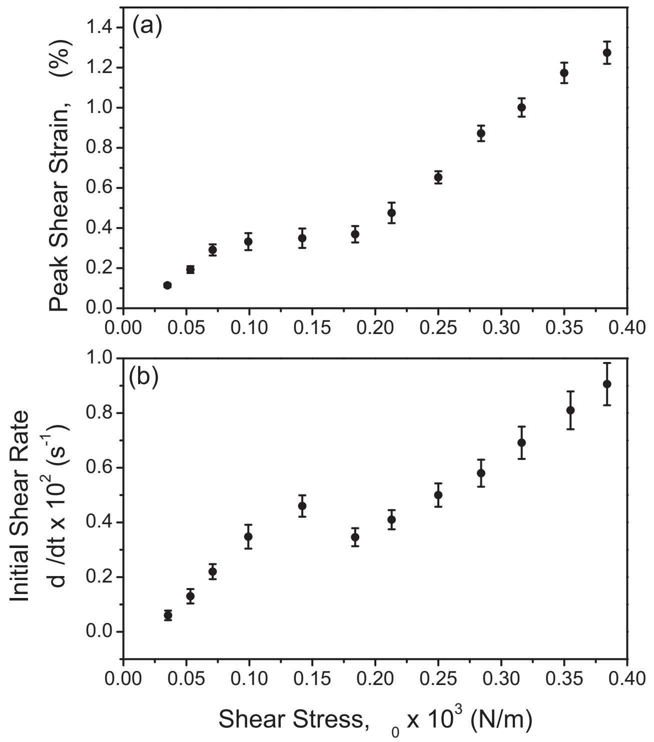

Fig. 5. (a) Peak strain maxima as function of the applied shear stress. The peak strain magnitude corresponded to the maximum strain value as estimated from the oscillatory response in Fig. 3. (b) Initial shear rate as a function of the applied shear stress.

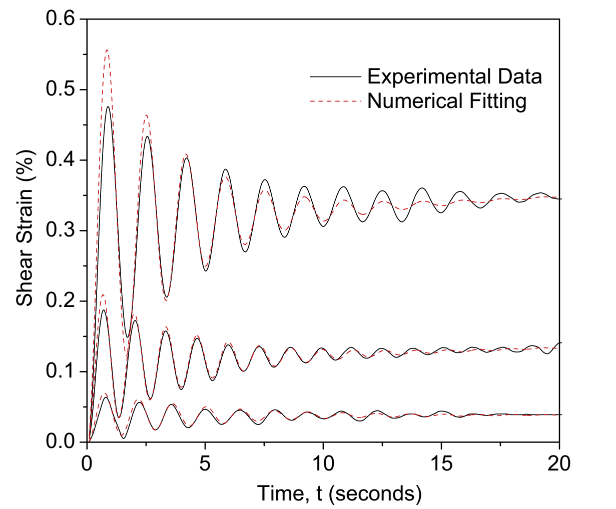

Fig. 6. Experimental data and the corresponding numerical least-square fitting for the KV model given by Eq. (1) for the three constant shear stresses shown in Fig. 4. The KV model with inertia was able to exhibit damped oscillations with acceptable fitting of the experimental data.

by quickly adapting its microstructure to the disturbance conditions. The oscillatory response was the way by which the compactly packed starch dispersion responded for avoiding fracture by dissipating mechanical energy. Fig. 4 also shows that the oscillatory shear strain response was not longer exhibited when the compactly packed ghost structure was partially destroyed. In fact, the application of short-time sonication induced isolated regions where the ghost remnants were concentrated (see Fig. 2c and d). It is apparent that this led to weakened elastic interactions between starch ghosts, and consequently to a response dominated by the viscous dissipation mechanism as induced by the amylose-rich continuous matrix.

Fig. 5a presents the magnitude of the peak strain maxima as a function of the applied shear stress. The peak strain–stress relationship increased monotonously, which reflects the fact that large shear stress led to large shear strain response. Interestingly, the strain–stress relationship was nonlinear, exhibiting three different behaviours that can be described as follows: (a) for small shear stress values, less than about 0.075×10^{-3} N/m, the behaviour was nearly linear, which can reflect a compaction of ghost granules into the gelatinized amylose matrix; (b) in the range from 0.075×10^{-3} to 0.2×10^{-3} N/m, the response was nearly flat (i.e., the yield was reduced), indicating that a further shear stress application hardly increased the material displacement. It is suggested that this behaviour could reflect the sticking together of ghosts within the gelatinized continuous matrix, opposing in this way a resistance to deformation; and (c) after a critical shear stress value, about 0.2×10^{-3} N/m, the strain–stress relationship increased again, and the magnitude of the shear stress was such that the breakage of the compact microstructure occurred accompanied by large deformations of the ghost granules in the direction of the flow field.

A shear rate–strain relationship can be computed by estimating the slope of the shear strain response for small times. To this end, the initial slope of the response curve was estimated by using central finite-differences coupled with $\alpha\beta$-filtering for reducing the effects of measurement noise (Echeverrıa et al., 2003). The results are presented in Fig. 5b, showing the presence of a non-monotonous behaviour with a folding that coincides with the plateau of the strain–stress relationship in Fig. 5a. This structure suggests that granule remnants suffered a rearrangement within the viscous, amylose-rich matrix. As commented above, such microstructural change could be related to the sticking together of the ghosts, leading to a more compact spatial distribution.

3.4. Phenomenological modelling

The strain response experimental data in Fig. 4 showed the occurrence of a phenomenon known as creep ringing (i.e., damped oscillatory behaviour). Dynamics of this type are known as inertio-elastic oscillations, occurring frequently in rotational rheometry as a consequence of a material's elasticity and the inertia of the rheometer (Yao, Larsen, & Weitz, 2008). In terms of mechanical analogies, oscillatory dynamics cannot be exhibited by first-order ordinary differential equations, requiring a second-order equation at least. In this way, Kelvin–Voigt (KV) models complemented with the addition of an inertial Newtonian effect can be used for explaining rheometer-material viscoelastic interactions as follows (Carrillo-Navas, Pérez-Alonso, Fouconnier, Vernon-Carter, & Alvarez-Ramirez, 2014):

$$m_{KV}\frac{d^2\gamma}{dt^2} + \mu_{KV}\frac{d\gamma}{dt} + E_{KV}\gamma = \sigma_0 \quad (1)$$

with initial conditions $\gamma(0) = 0$, $d\gamma(0)/dt = \gamma'_0$. Here, γ is the shear strain, σ_0 is the applied shear stress, m_{KV} is the virtual mass (i.e., inertia) associated to the material displacement, μ_{KV} is the effective viscosity and E_{KV} is the elasticity modulus. The term $m_{KV}d^2\gamma/dt^2$ accounts for the acceleration effects introduced by the sudden step change in the shear stress σ, and these effects should be reflected mainly for relatively short shear times. For longer shear times, the acceleration effects are dissipated by the action of the viscosity (i.e., damping) component $\mu_{KV}(d\gamma/dt)$. For obtaining damped oscillatory dynamics with Eq. (1), the constraint $\mu_{KV}^2 - 4m_{KV}E_{KV} < 0$ should be satisfied. In fact, the quantity $\omega_{KV} = \sqrt{|\mu_{KV}^2 - 4m_{KV}E_{KV}|/2m_{KV}}$ represents the oscillation frequency while $\tau_{KV} = 2m_{KV}/\mu_{KV}$ is the damping (i.e., relaxation) time constant.

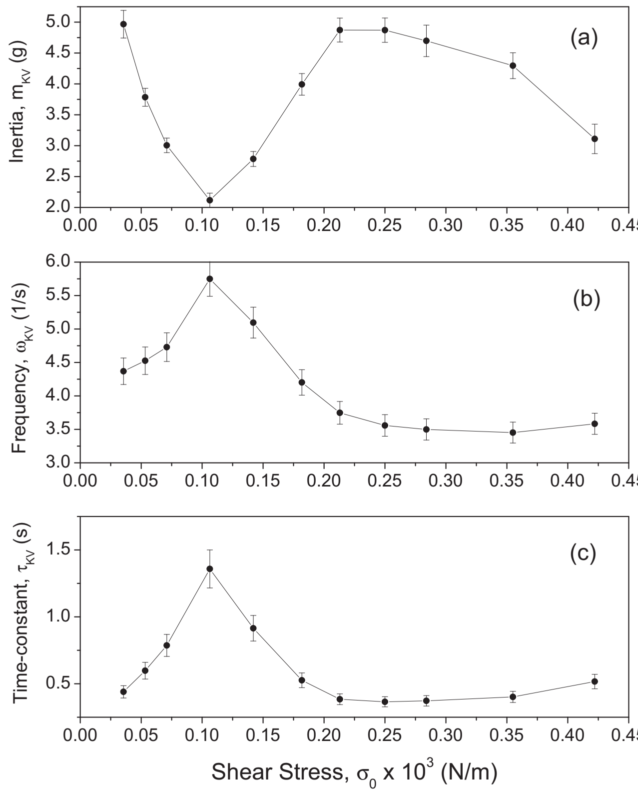

Fig. 7. Behaviour of the model parameters: (a) Inertia, (b) characteristic frequency, and (c) characteristic time-constant, as function of the applied shear stress σ_0. A maximum in the oscillation frequency and time-constant indicated that the GSD was subjected to nonlinear microstructural changes even at very low deformations.

Fig. 6 compares the experimental data and the corresponding numerical least-square fitting for the KV model given by Eq. (1) for the three experimental data shown in Fig. 4. The KV model with inertia was able to exhibit damped oscillations with acceptable fitting of the experimental data. Some fitting deviations can be observed for the initial and the final oscillations, mainly for large shear stress values. This inaccurate fitting could be caused by nonlinear dynamical effects acquiring importance at large material deformations. In general, the second-order model was able to describe the inertio-oscillatory phenomena over the scrutinized range of shear stress values. Fig. 7 presents the behaviour of the model parameters $\{m_{KV}, \tau_{KV}, \omega_{KV}\}$ as functions of the applied shear stress, σ_0. All the parameters exhibited variations with σ_0, suggesting that nonlinearities were affecting the rheological response of the GSD. It is apparent that the parameter variations reflected the lack of a linear region in the strain sweep pattern for small deformation values in Fig. 3. In fact, the presence of a linear regime should imply that the oscillation frequency and time-constant were nearly constant over the studied shear stress domain. In contrast, the model parameters exhibited important variations that could be related to changes of the GSD microstructure as the shear stress was increased. Two regions can be distinguished in the behaviour of the oscillation parameters: (a) for $\sigma_0 > 0.2 \times 10^{-3}$ N/m, both ω_{KV} and τ_{KV} were nearly constant, indicating linear viscoelastic behaviour. It is noted that the inertia m_{KV} decreased in this region, indicating that the apparent linear regime was obtained when the viscous effects dominated over the inertial ones as the shear stress was increased beyond the threshold of $\sigma_0 = 0.2 \times 10^{-3}$ N/m. (b) For $\sigma_0 < 0.2 \times 10^{-3}$ N/m, the oscillation frequency and time-constant presented respectively a maximum and a minimum at about $\sigma_0 = 0.1 \times 10^{-3}$ N/m. This suggests that the GSD underwent microstructural changes as the shear stress was increased. Interestingly, the region of the minimum/maximum of the estimated parameters coincides with the plateau region in the peak strain–stress and the folding of the initial shear rate–stress curves exhibited in Fig. 5a and b, respectively. The maximum of the oscillation frequency indicated that mechanical waves induced by strain oscillations propagated faster in the GSD bulk, which is in line with the reduced yield as represented by the plateau region in the peak strain–stress curve (Fig. 5). Also, the nonlinear pattern of the inertio-elastic oscillation parameters can be linked to the small overshoot exhibited by the strain sweep tests exhibited in Fig. 3. As mentioned before, such strain overshoot could be related to a compaction of ghost granules into the gelatinized amylose matrix, as induced by small shear strains.

4. Conclusions

This work explored the viscoelastic behaviour of corn gelatinized starch dispersions in the presence of inertio-elastic oscillations. To this end, the mechanical response under strain sweeps and small shear stress steps was obtained experimentally. Strain sweeps showed the presence of an overshoot in the loss modulus behaviour, suggesting the presence of nonlinear effects in the viscoelasticity behaviour for relatively small gel deformations. The application of small shear stress values resulted in oscillatory shear strain response, indicating that inertial effects played an important role in the starch mechanical response. Phenomenological modelling incorporating inertial acceleration showed good fitting of experimental data, from which the dominant oscillation frequency and time-constant values were estimated. It was shown that the oscillation parameters exhibited important variations with the shear stress, which were related to changes (e.g., compact packing and fracture of ghosts) in the gel microstructure. Overall, the results in this work showed that nonlinearities (e.g., nonlinear stress–strain relationship) were not only found for large gel deformations, where the gel microstructure is subjected to large fractures, but also at relative small deformations (∼1%), where the gel undergoes microstructural adaptations to changing shear stress conditions. The present results can provide important insights in the behaviour of food products incorporating GSD under shelf and consumption conditions, for which relatively low shear stress values are used.

References

Atkin, N. J., Abeysekera, R. M., Cheng, S. L., & Robards, A. W. (1998). An experimentally-based predictive model for the separation of amylopectin subunits during starch gelatinization. *Carbohydrate Polymers*, *36*, 173–192.

Biliaderis, C. G., Maurice, T. J., & Vose, J. R. (1980). Starch gelatinization phenomena studied by differential scanning calorimetry. *Journal of Food Science*, *45*(6), 1669–1674.

Bremer, L. G. B., Bijsterbosch, B. H., Waltra, P., & van Vliet, T. (1993). Formation, properties and fractal structure of particle gels. *Advances in Colloid and Interface Science*, *46*, 117–128.

Carini, E., Curti, E., Littardi, P., Luzzini, M., & Vittadini, E. (2013). Water dynamics of ready to eat shelf stable pasta meals during storage. *Innovative Food Science & Emerging Technologies*, *17*, 163–168.

Carrillo-Navas, H., Fouconnier, B., Vernon-Carter, E. J., & Alvarez-Ramirez, J. (2013). Shear rheology of water/glycerol monostearate crystals in canola oil dispersions interfaces. *Colloids and Surfaces A: Physicochemical and Engineering Aspects*, *436*, 215–224.

Carrillo-Navas, H., Pérez-Alonso, C., Fouconnier, B., Vernon-Carter, E. J., & Alvarez-Ramirez, J. (2014). Inertial effects of adsorbed glycerol monostearate crystals on the shear rheology of water/canola oil interfaces. *Journal of Food Engineering*, *125*, 112–118.

Cui, B., Lu, Y. M., Tan, C. P., Wang, G. Q., & Li, G. H. (2014). Effect of cross-linked acetylated starch content on the structure and stability of set yoghurt. *Food Hydrocolloids*, *35*, 576–582.

Debet, M. R., & Gidley, M. J. (2007). Why do gelatinized starch granules not dissolve completely? Roles for amylose, protein, and lipid in granule ghost integrity. *Journal of Agricultural and Food Chemistry*, *55*, 4752–4760.

Echeverrıa, J. C., Woolfson, M. S., Crowe, J. A., Hayes-Gill, B. R., Croaker, G. D. H., & Vyas, H. (2003). Interpretation of heart rate variability via detrended fluctuation

analysis and αβ filter. *Chaos: An Interdisciplinary Journal of Nonlinear Science*, *13*, 467–475.
Fannon, J. E., & BeMiller, J. N. (1992). Structure of corn starch paste and granule remnants revealed by low-temperature scanning electron microscopy after cryopreparation. *Cereal Chemistry*, *69*, 456–460.
Ghiasi, K., Hoseney, R. C., & Varriano-Marston, E. (1982). Gelatinization of wheat starch. III. Comparison by differential scanning calorimetry and light microscopy. *Cereal Chemistry*, *59*, 258–264.
Hernández-Jaimes, C., Bello-Pérez, L. A., Vernon-Carter, E. J., & Alvarez-Ramirez, J. (2013). Plantain starch granules morphology, crystallinity, structure transition, and size evolution upon acid hydrolysis. *Carbohydrate Polymers*, *95*, 207–213.
Hoover, R., & Ratnayake, W. S. (2002). Starch characteristics of black bean, chick pea, lentil, navy bean and pinto bean cultivars grown in Canada. *Food Chemistry*, *78*, 489–498.
Hoseney, R. C., Atwell, W. A., & Lineback, D. R. (1977). Scanning electron microscopy of starch isolated from baked products. *Cereal Foods World*, *22*, 56–63.
Hyun, K., Kim, S. H., Ahn, K. H., & Lee, S. J. (2002). Large amplitude oscillatory shear as a way to classify the complex fluids. *Journal of Non-Newtonian Fluid Mechanics*, *107*, 51–65.
Hyun, K., Wilhelm, M., Klein, C. O., Cho, K. S., Nam, J. G., Ahn, K. H., et al. (2011). A review of nonlinear oscillatory shear tests: Analysis and application of large amplitude oscillatory shear (LAOS). *Progress in Polymer Science*, *36*, 1697–1753.
Lourdin, D., Valle, G. D., & Colonna, P. (1995). Influence of amylose content on starch films and foams. *Carbohydrate Polymers*, *27*, 261–270.
Luyten, H., & van Vliet, T. (1995). Fracture properties of starch gels and their rate dependency. *Journal of Texture Studies*, *26*, 281–298.
Martin, A., Bos, M., Stuart, M. C., & van Vliet, T. (2002). Stress–strain curves of adsorbed protein layers at the air/water interface measured with surface shear rheology. *Langmuir*, *18*, 1238–1243.
McClements, D. J. (1999). *Food emulsions: Principles, practice and techniques*. Boca Raton, FL: CRC Press (Chapter 8).
Muadklay, J., & Charoenrein, S. (2008). Effects of hydrocolloids and freezing rates on freeze–thaw stability of tapioca starch gels. *Food Hydrocolloids*, *22*, 1268–1272.
Pal, R. (1996). Rheology of emulsions containing polymeric liquids. In P. Becher (Ed.), *Encyclopedia of emulsion technology* (Vol. 4) (pp. 93–264). New York: Marcel Dekker.
Ratnayake, W. S., & Jackson, D. S. (2007). A new insight into the gelatinization process of native starches. *Carbohydrate Polymers*, *67*, 511–529.
Rochefor, W. E., & Middleman, S. (1987). Rheology of xanthan gum: Salt, temperature, and strain effects in oscillatory and steady state shear experiments. *Journal of Rheology*, *31*, 337–369.
Seetapan, N., Fuongfuchat, A., Gamonpilas, C., Methacanon, P., Pongjaruwat, W., & Limparyoon, N. (2013). Effect of modified tapioca starch and xanthan gum on low temperature texture stability and dough viscoelasticity of a starch-based food gel. *Journal of Food Engineering*, *119*, 446–453.
Sim, H. G., Ahn, K. H., & Lee, S. J. (2003). Large amplitude oscillatory shear behavior of complex fluids investigated by a network model: A guideline for classification. *Journal of Non-Newtonian Fluid Mechanics*, *112*, 237–250.
Yao, N. Y., Larsen, R. J., & Weitz, D. A. (2008). Probing nonlinear rheology with inertio-elastic oscillations. *Journal of Rheology*, *52*, 1013–1025.
Zhang, B., Dhital, S., Flanagan, B. M., & Gidley, M. J. (2014). Mechanism for starch granule ghost formation deduced from structural and enzyme digestion properties. *Journal of Agricultural Food Chemistry*, *62*, 760–771.